Acta Cryst. (1973). B**29**, 1991

Crystal Structure and Linear Thermal Expansivities of Platinum Silicide and Platinum Germanide*

BY E. J. GRAEBER, R. J. BAUGHMAN AND B. MOROSIN

Sandia Laboratories, Albuquerque, New Mexico 87115, *U.S.A.*

(*Received* 11 *April* 1973; *accepted* 5 *May* 1973)

Positional and thermal parameters for PtSi and PtGe have been refined by the full-matrix least-squares method using 123 and 131 three-dimensional intensity data, respectively. The compounds are isostructural with MnP, space group *Pbnm*, four formulae per cell, with lattice constants $a=5{\cdot}916$ (1), $b=5{\cdot}577$ (1), $c=3{\cdot}587$ (1) Å for PtSi, and $a=6{\cdot}084$ (2), $b=5{\cdot}719$ (2), $c=3{\cdot}697$ (1) Å for PtGe. Linear thermal expansivities have been determined from the lattice constants measured as a function of temperature over the interval 100–900 °K for PtSi and 298–900 °K for PtGe. An anomaly in the expansivities for PtSi occurs at 400 °K.

Introduction

The nature of the electronic structure of PtSi is of considerable interest since the resistivity is near the value for platinum metal. Recent magnetic measurements of the bulk susceptibility and n.m.r. parameters (Weaver, Knauer, Quinn & Baughman, 1972) have provided information regarding the nature of the conduction electrons. Interestingly, the appearance of two overlapping peaks in the ^{195}Pt n.m.r. spectra is not consistent with the published structure of PtSi (Pfisterer & Schubert, 1950: hereafter P & S) which possesses only one symmetry site for Pt. Diffraction photographs to determine the correctness of the space group were taken below, at and above room temperature in order to corroborate the n.m.r. results; however, these photographs were found to be consistent with the results of P & S. Furthermore, these photographs suggested that the value of the linear thermal expansivity along the *c* axis greatly differed from those along the other two axes. On the basis of powder data, P & S indicated that the crystal structure parameters for PtGe are identical to those for PtSi and that both structures belong to the MnP-type, a distortion of the NiAs-type structure. The redetermination of the room-temperature structure parameters and the linear thermal expansivities on PtSi and PtGe are reported here.

Experimental

Small single-crystal spheres were grown by a technique developed by one of the authors (Baughman, 1972). Lattice constants for PtSi [$a_o=5{\cdot}916$ (1), $b_o=5{\cdot}577$ (1), $c_o=3{\cdot}587$ (1) Å] and PtGe [$a_o=6{\cdot}084$ (2), $b_o=5{\cdot}719$ (2), $c_o=3{\cdot}697$ (1) Å] were obtained by a least-squares fit of high 2θ reflections [Cu $K\alpha$ radiation (λ for $K\alpha_1=1{\cdot}54051$ Å)]; these 2θ values were determined on a Picker diffractometer and with a 115 mm diameter Straumanis loaded Weissenberg camera. The symmetry of the reciprocal lattice was recorded by the Weissenberg and precession methods; very long exposures were taken at ~250, 298 and 450 °K in order to reconcile the interpretation of the ^{195}Pt n.m.r. spectra as well as the slight thermal expansion anomaly described below. Systematic absences of $h0l$ reflections for $h+l$ odd, $0kl$ for k odd indicate the space group to be $Pbn2_1$ or *Pbnm* as determined by P & S. The two isomorphous compounds contain 4 formulae per cell; densities obtained by a Berman torsion balance of 12·36 and 13·76 g cm^{-3} are in good agreement with calculated values of 12·53 and 13·82 g cm^{-3} for PtSi and PtGe, respectively.

The θ–2θ scan technique and a scintillation detector employing pulse-height discrimination were used to measure the Mo $K\alpha$ intensity data on single-crystal spheres mounted on [010]. Four symmetry-related sets for positive values of k were examined for differences among hkl and $hk\bar{l}$ that might suggest the noncentrosymmetric *Pbn*2 structure. Among the four individual sets of observed intensities, no consistent discrepancies were noted that would indicate a space group other than *Pbnm*. Unique data sets for the two compounds were obtained by averaging intensities from the four equivalent sets provided the differences were less than $\sigma_{ave}/\sqrt{n}$, where σ_{ave} is the average σ for n measurements with the usual definition of $\sigma=(N_{Sc}+K^2N_B)^{1/2}$, where N_{Sc}, N_B and K are the total scan count, background counts and the ratio of the scan to background counts, respectively. In the few instances where an intensity did not agree with this criterion, it was discarded and the averaging was performed on the remaining three intensities. For PtSi 123 intensities were measured, of which 31 were considered to be unobserved; for PtGe 131 were measured and 8 considered unobserved. Extrapolated spherical absorption corrections [PtSi/PtGe; μ(Mo $K\alpha$) = 1307·0/1438·0 cm^{-1}; crystal diameter = 0·203/0·178 mm] were applied to each data set from

* This work was supported by the U.S. Atomic Energy Commission.

Table 5.3.6B of *International Tables for X-ray Crystallography* (1959). The spherical deviation of the crystals measured on an optical comparator did not exceed 2%.

The lattice constants as a function of temperature were initially obtained over the temperature interval 298–900°K. The values at a particular temperature were determined by a least-squares fit of 2θ values (13 for PtSi, 16 for PtGe) in the range 140–160° 2θ using Cu $K\alpha$ radiation. The single crystals were mounted in a high-temperature X-ray diffraction furnace described elsewhere (Lynch & Morosin, 1971). When it was found that for PtSi a slight anomaly occurred near 423°K, data were obtained below 295°K by cooling the crystal specimen with flowing N_2 gas. The lattice constants for PtSi as a function of temperature are shown in Fig. 1. Similar data for PtGe are not shown, since the thermal expansivities are linear in the range 298–900°K.

Refinement and results

Starting with the positional parameters determined by P & S, the data sets were subjected to full-matrix least-squares refinement using anisotropic thermal parameters. The function $\sum w(F_o-F_c)^2$ was minimized; weights are assigned from counting statistics ($w=n/\sigma_{ave}^2$) or set to zero for unobserved reflections when $F_o<F_c$. Structure factors were calculated with Pt, Si and Ge scattering factors taken from Tables 3.3.1A and 3.3.1B and dispersion corrections from Table 3.3.2C of *International Tables for X-ray Crystallography* (1962). Isotropic extinction corrections were employed and the residual, $R=\sum||F_o|-|F_c||/\sum|F_o|$, was 0·018 and 0·061 for PtSi and PtGe data sets, respectively.

The positional and thermal parameters for each compound are given in Table 1. Observed and calculated structure factors obtained with these parameters are given in Table 2. A projection of the crystal structure of the compounds as viewed along the c axis is represented in Fig. 2. In this MnP-type structure, each silicon (or germanium) atom is surrounded by six platinum atoms at the corners of a distorted trigonal prism (Table 3, distances E, F and G). [In NiAs, the corresponding atom (arsenic) is also not required by symmetry to be centered within the regular trigonal prism.] One base (distances G and c axis, see Fig. 2) is considerably larger than the other (distances F and c axis). Platinum atoms are coordinated to six silicon (or germanium) atoms at the corners of a distorted octahedron, and to four platinum atoms which are tetrahedrally distributed in four of the octahedral interstices. (An interesting feature of separation E is that in the NiAs-type structure it is significantly smaller, as will be discussed below.)

In both compounds, the platinum B_{11} thermal parameter appears to be significantly smaller than B_{22} or B_{33}; however, consideration of the interatomic separations does not provide any qualitative arguments for such a result.

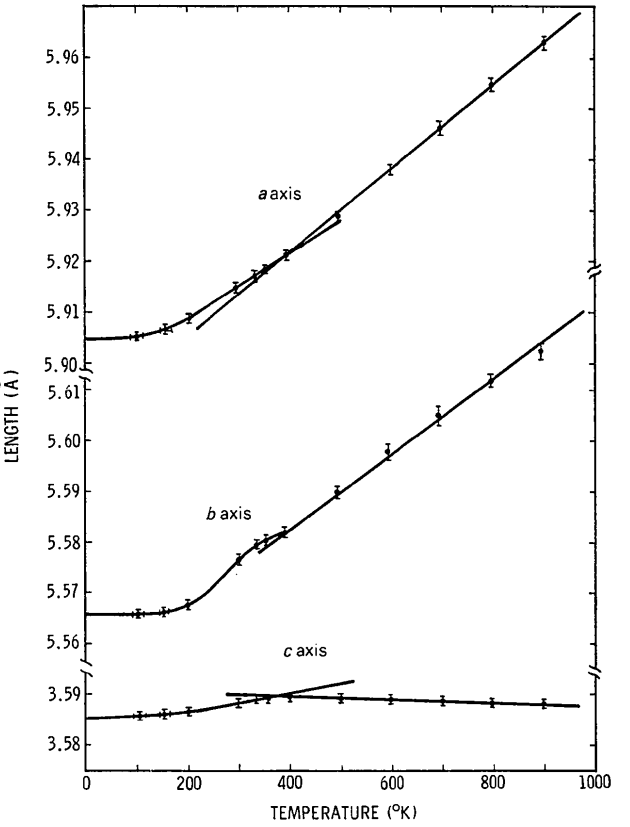

Fig. 1. PtSi lattice constants as a function of temperature.

Table 1. *Atomic positional and anisotropic thermal parameters for* PtSi *and* PtGe

Thermal parameters are of the form: $\exp(-\frac{1}{4}\sum\sum B_{ij}h_ih_ja_i^*a_j^*)$; by symmetry, $B_{13}=B_{23}=0$. Standard deviations are given in parentheses, values from Pfisterer & Schubert (1950) in square brackets.

	x	y	z	B_{11}	B_{22}	B_{33}	B_{12}
Pt	0·1922 (1)	−0·0044 (2)	¼	0·57 (6)	0·79 (6)	0·94 (6)	0·07 (3)
	[0·195]	[0·010]	[¼]				
Si	0·583 (1)	0·177 (1)	¼	0·9 (2)	1·1 (2)	1·2 (2)	−0·1 (2)
	[0·590]	[0·195]	[¼]				
Pt	0·1908 (4)	−0·0005 (4)	¼	0·6 (1)	1·1 (1)	1·1 (1)	−0·08 (7)
	[0·195]	[0·010]	[¼]				
Ge	0·590 (1)	0·185 (1)	¼	0·4 (2)	0·8 (3)	0·9 (3)	−0·1 (2)
	[0·590]	[0·195]	[¼]				

Table 2. *Observed and calculated structure factors for* PtSi (*left*) *and* PtGe

Unobserved reflections are marked with an asterisk. F_o and F_c are both $\times 10$.

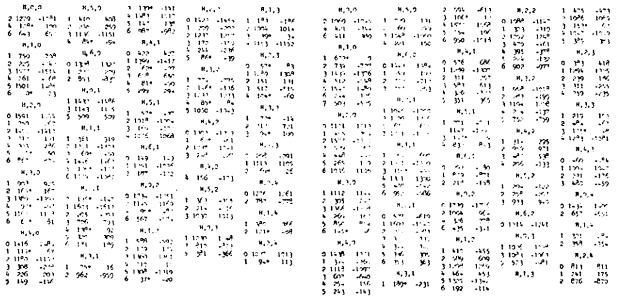

Table 3. *Interatomic separations and deviations for* PtSi *and* PtGe

Letters in parentheses refer to separations shown in Fig. 1.

	PtSi		PtGe
Pt–Si	(*A*) 2·407 (7) Å	Pt–Ge	(*A*) 2·480 (6) Å
	(*B*) 2·434 (5)		(*B*) 2·512 (4)
	(*C*) 2·523 (7)		(*C*) 2·649 (6)
	(*D*) 2·638 (5)		(*D*) 2·656 (5)
Pt–Pt	(*E*) 2·871 (1)	Pt–Pt	(*E*) 2·949 (3)
	(*F*) 2·896 (1)		(*F*) 2·968 (2)
	(*G*) 4·060 (1)		(*G*) 4·192 (2)
Si–Si	(*H*) 2·844 (8)	Ge–Ge	(*H*) 3·013 (7)

Numerical calculations on the refinement of the structures were performed on a CDC-6600 computer using the X-RAY 71 system of crystallographic programs (Stewart, 1971).

Linear thermal expansivities ($\beta_a = \partial \ln a / \partial T$) were determined from values of the lattice parameters as a function of temperature. For PtSi, the values along the *a*, *b*, and *c* axes in the temperature interval 400–900 °K are 15·9, 13·2 and $-1{\cdot}3$ (all $\times 10^{-6}$ °K^{-1}), respectively; below 400 °K to ~220 °K the *c*-axis expansivity is linear and positive ($4{\cdot}6 \times 10^{-6}$ °K^{-1}), the *a*-axis expansivity is linear ($11{\cdot}0 \times 10^{-6}$ °K^{-1}), while the *b*-axis undergoes a slight nonlinear behavior; all three axes show some anomaly at ~400 °K. For PtGe, the expansivities are linear in the temperature range 298–900 °K. The values are 6·84, 6·10 and 1·13 (all $\times 10^{-6}$ °K^{-1}), along the *a*, *b* and *c* axes, respectively.

Careful examination of photographs taken at room temperature and ~450 °K did not reveal any changes in symmetry or significant changes in intensities. The small anomaly at 400 °K in PtSi is not understood and probably results from a delicate balance of crystal forces between neighbors, the dominant role evidently passing to a different set of crystal forces. The MnP-type structure is inconsistent with the two-line n.m.r. spectra which have been initially reported. Since our single-crystal specimens are prepared by a different procedure, surface inhomogeneities are possibly playing a more important role than previously recognized in the n.m.r. samples.

Comparison of PdX and PtX compounds (Wyckoff, 1963) where X = Si, Ge, Sn and Sb, shows several interesting trends. In Table 4, isomorphous compounds of the MnP-type are listed together with the hexagonal NiAs-type, the MnP-type being related to the NiAs-type by a slight distortion. The order selected for the compounds in Table 4 is the volume per atom exhibited by the room-temperature lattice constants. Examination of the ratio of atomic radii, M/X [the metallic radii of Pauling (1960) are arbitrarily selected although ionic or covalent radii are also valid] suggests a transition between MnP- and NiAs-types near a value of 1·0. This fact implies that the smaller radii of X atoms allows the regular NiAs structure to collapse to that of the more distorted MnP arrangement. The departure from the ideal hexagonal cell ($\sqrt{3}$) can be seen from values of *a*/*c* (orthorhombic) which cover a range 6% smaller to 5% larger than ideal. Note that the departure for PtSi and PtGe is in an opposite direction from that for PdSi and PdGe. Coupled with this departure from ideality is the relative increase of the orthorhombic *b* axis which is sufficiently large that MnP-type compounds possess axial ratios of $\sqrt{3}b/a$ and *b*/*c* which are much larger (1·55–1·68) than the corresponding hexagonal *c*/*a* ratio (1·32–1·37) for the NiAs-type compounds. In fact, for the NiAs-type compounds, the metal–metal separations along the *c* axis (*c*/2) are rather short and correspond to a distance less than that predicted from values of metallic radii. An additional trend is observed on comparing axial ratios between corresponding sets of Pd and Pt compounds; the *c* axis of PdSb is longer than that of PtSb and the trend is preserved with the MnP-type structures (the ortho-

Table 4. *Comparison of lattice constants for* PdX *and* PtX *compounds*

	a	*b*	*c*	*V*/atom	*R*	*a*/*c*	$\sqrt{3}b/a$	*b*/*c*
PdSi	6·133 Å	5·599 Å	3·381 Å	14·51 Å^3	1·09	1·814	1·600	1·661
PtSi	5·916	5·577	3·587	14·79	1·10	1·649	1·633	1·555
PdGe	6·259	5·782	3·481	15·75	1·03	1·798	1·600	1·661
PtGe	6·084	5·719	3·697	16·08	1·04	1·646	1·628	1·547
PdSn	6·32	6·13	3·87	18·74	0·90	1·633	1·680	1·584
PtSn	4·103		5·428	19·79	0·91	$\sqrt{3}$*		1·323*
PdSb	4·070		5·582	20·03	0·92	$\sqrt{3}$*		1·372*
PtSb	4·130		5·472	20·22	0·93	$\sqrt{3}$*		1·325*

* Column headings are for orthorhombic axes; for the hexagonal compounds the corresponding lengths would be a/d_{100} and *c*/*a*, respectively.

rhombic *b* axis corresponds to the hexagonal *c* axis).

Although thermal expansivities are presented for only two members of the MnP-type compounds, the very low value along the *c* axis in comparison with that along the *a* axis for both compounds is consistent with the hypothesis that structures tend towards more symmetric arrangements of constituents with increasing temperature (Cartz, 1968; Li & Peacor, 1968).

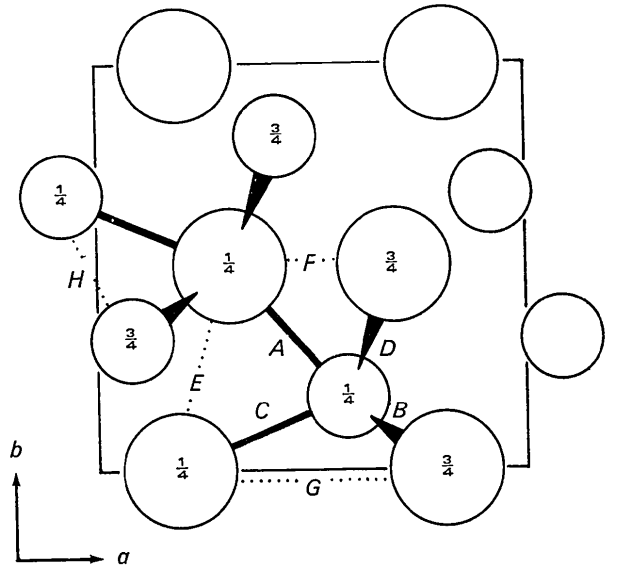

Fig. 2. A projection of PtSi and PtGe structures along the *c* axis; fractional heights indicated above projection plane; platinum atoms are represented as the larger circles.

The assistance of Mrs P. G. Neiswander and Mr R. A. Trudo is gratefully acknowledged.

References

BAUGHMAN, R. J. (1972). *Mater. Res. Bull.* **7**, 1–4.
CARTZ, L. (1968). In *Anisotropy in Single-Crystal Refractory Compounds*, Vol. I, pp. 383–398, edited by F. W. VAHLDIEK and S. A. MERSOL. New York: Plenum Press.
International Tables for X-ray Crystallography (1959). Vol. II. Birmingham: Kynoch Press.
International Tables for X-ray Crystallography (1962). Vol. III. Birmingham: Kynoch Press.
LI, C. T. & PEACOR, D. R. (1968). *Z. Kristallogr.* **126**, 46–65.
LYNCH, R. W. & MOROSIN, B. (1971). *J. Appl. Cryst.* **4**, 352–356.
PAULING, L. (1960). *The Nature of the Chemical Bond.* Ithaca: Cornell Univ. Press.
PFISTERER, H. & SCHUBERT, K. (1950). *Z. Mettalk.* **41**, 358–367.
STEWART, J. M. (1971). The X-ray System of Crystallographic Programs, Computer Science Center, Univ. of Maryland.
WEAVER, H. T., KNAUER, R. C., QUINN, R. K. & BAUGHMAN, R. J. (1972). *Solid State Commun.* **11**, 453–455.
WYCKOFF, R. W. G. (1963). *Crystal Structures*, Vol. I. New York: John Wiley.

Acta Cryst. (1973). B**29**, 1994

Structure Cristalline de Composés Antituberculeux. IV.* Structure Cristalline de l'Ethyl-2 Thiocarbamoyl-4 Pyridine

PAR M. ALLÉAUME ET F. LEROY

Laboratoire de Cristallographie au CNRS, Faculté des Sciences, Université de Bordeaux I, 351 *cours de la Libération*, 33405 *Talence, France*

ET M. GADRET ET M. GOURSOLLE

Laboratoire de Cristallographie, Faculté de Pharmacie, Université de Bordeaux II, *Rue Leyteire*, 33000 *Bordeaux, France.*

(*Reçu le* 9 *mars* 1973, *accepté le* 27 *avril* 1973)

2-Ethyl-4-thiocarbamoylpyridine ($C_8N_2H_{10}S$) crystallizes in the monoclinic system, space group *Cc*, with cell dimensions $a=8{\cdot}832$ (2), $b=14{\cdot}996$ (4), $c=7{\cdot}918$(2) Å, $\beta=128{\cdot}51$ (5)° and 4 molecules per cell. The refinement was carried out by least-squares calculations including anisotropic temperature factors. The final *R* value is 0·0292. The structure is made up of chains of molecules parallel to the (100) plane; the molecules are linked together by hydrogen bonds.

Introduction

Ce dérivé est utilisé en médecine humaine sous forme de chlorhydrate, soluble dans l'eau, et sous forme basique.

Nous avons, dans une précédente note (Colleter & Gadret, 1968), rapporté la structure du chlorhydrate. C'est donc celle de la forme basique que nous nous proposons de décrire (Fig. 1).

Partie expérimentale

L'éthyl-2 thiocarbamoyl-4 pyridine cristallise très facilement dans différents solvants. Les cristaux utilisés

* Partie III: *Acta Cryst.* (1970). B**26**, 151–1518.